Analysis of a Class of Cylindrical Multiconductor Transmission Lines Using an Iterative Approach

CHI HOU CHAN, MEMBER, IEEE, AND RAJ MITTRA, FELLOW, IEEE

Abstract—**A class of cylindrical multiconductor transmission lines is theoretically analyzed, and useful parameters, e.g., characteristic impedance and effective dielectric constant, are derived. Discretization of the continuous functions and exploitation of the periodicity of the cylindrical structure lead to a discrete convolution which can be carried out numerically rigorously and efficiently using the FFT algorithm. An iterative technique is employed in the spectral domain to derive the solution of integral equations for the charge distribution. Numerical results are presented and compared with available data.**

I. Introduction

CYLINDRICAL STRIPLINES and microstrip lines operating in the quasi-TEM mode have recently received much attention in the microwave literature [1]–[6]. Using flexible dielectrics, it is possible to construct nonplanar transmission lines that can be wrapped around a cylindrical surface and used to excite conformal arrays mounted on a cylindrical object. A cylindrical transmission line is also useful for modeling a warped, planar transmission line that has been subjected to severe environmental changes.

Two basic approaches have been employed to analyze cylindrical striplines and microstrip lines. The first of these entails the solution of the Laplace equation in cylindrical coordinates and yields a dual series representation for the potential function. The constants appearing in the series are obtained either by using the least-square or simple integration methods [1] or by solving two simple equations that take the fringing field into account [6]. In this method, the analysis is not rigorous because the infinite series is truncated. The second approach transforms the cylindrical structure into a planar one by conformal mapping [3]–[5]. Although this method is rigorous, the solution requires the numerical evaluation of elliptical integrals. In any event, neither of these two approaches is suitable for the analysis of cylindrical multiconductor transmission lines.

In this paper, a class of cylindrical multiconductor transmission lines is analyzed using a spectral-domain formulation. The continuous functions representing the charge distribution are discretized into a series of cylindrical pulses with unknown weighting coeffients. Next, these coefficients are solved for using an iterative procedure [7]–[9] appropriate for the spectral-domain formulation. Unlike the planar structures [8] that are aperiodic in the transverse direction, the cylindrical transmission lines are strictly periodic in the ϕ direction; hence, the fast Fourier transform algorithm can be rigorously applied to compute the convolution integral [10]. For the single-conductor case, the characteristic impedances of a cylindrical stripline and microstrip line are compared with the results presented in [1], [2], [5], and [6]. Next, the finite-thickness strip is treated using a modified spectral Green's function [11], and the results for this geometry are compared with the data calculated from the equations provided in [5]. The iterative method is then extended to the two-conductor case, for which the even- and odd-mode characteristic impedances [12] are calculated. The propagation constants for different propagating modes of the cylindrical multiconductor transmission lines are also computed and displayed as a function of certain geometrical parameters.

II. Outline of Theoretical Procedure

The cross section of a generic cylindrical multiconductor transmission to be analyzed is shown in Fig. 1. With appropriate choices of parameters and boundary conditions, this structure can be reduced to a single-layer or multilayer stripline; a microstrip line; or a buried microstrip line. The Maxwell's coefficients of capacitance for the line can be readily obtained if the charge distribution on the conducting lines is known for different excitations. The line coefficients of inductance can be obtained from the coefficients of capacitance with the dielectric replaced by air [13]. The integral equation describing the problem can be written as

$$V(\phi,\rho_i)=\sum_j\int_{D_j}G_{ij}(\phi,\phi',\rho_i,\rho_j)\sigma_j(\phi',\rho_j)\,d\phi',\qquad \phi\in D_j \tag{1}$$

and

$$\sigma_j(\phi,\rho_j)=0,\qquad \phi\notin D_j \tag{2}$$

where D_j corresponds to the intervals in the ϕ direction

Manuscript received August 1, 1986; revised November 22, 1986. This work was supported in part by the Army Research Office under Grant DAAG 29-85-K-0183 and the Office of Naval Research under Grant N00014-85-K-0619.

The authors are with the Electromagnetic Communication Laboratory, Department of Electrical and Computer Engineering, University of Illinois, Urbana, IL 61801.

IEEE Log Number 8612956.

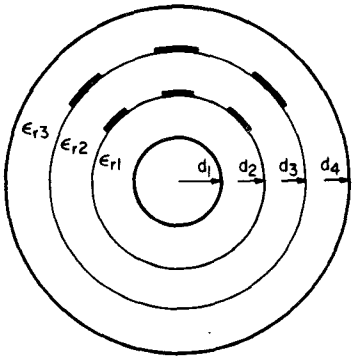

Fig. 1. Multiconductor cylindrical transmission line.

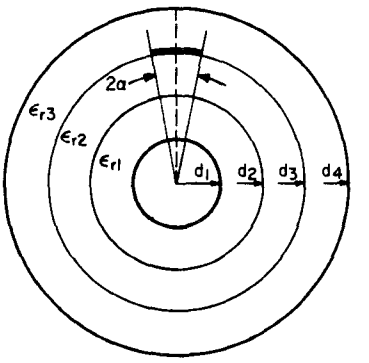

Fig. 2. Cylindrical stripline with a three-layer dielectric filling.

which coincide with the conducting strips on the jth interface occupied by the strips. $V(\phi, \rho_i)$ represents the specified voltages on the conducting strips and G_{ij} are the Green's functions to be determined in the next section. Then the only unknowns are the charge distributions $\sigma(\phi, \rho_j)$ on each of the conducting strips. For an N-conductor system, this integral equation is solved N times, corresponding to N independent excitations. The total charge on each of the strips is obtained by integrating the charge distribution along the arc length of the strip. The coefficients of capacitance $[C]$ and inductance $[L]$ are obtained through the following matrix equations:

$$Q = \int \sigma(\phi)\rho d\phi \tag{3}$$

$$[C] = [Q][V]^{-1} \tag{4}$$

$$[L] = \mu_0 \epsilon_0 [C_0]^{-1} \tag{5}$$

where $[V]$ is the voltage excitation matrix, $[Q]$ is the corresponding charge matrix, and $[C_0]$ is the capacitance matrix calculated with the dielectric layers replaced by air. The eigenvalues of the product of the $[L]$ and $[C]$ matrices will give the propagation velocities of the dominant propagating modes. These propagation velocities can then be converted to propagation constants for the cross-talk analysis of the transmission line.

III. Derivation of the Green's Function in the Spectral Domain

As a preamble to formulating the integral equation using the spectral-domain approach, we need to derive the spectral Green's function for the geometry under consideration. Initially, we assume that the strips are infinitely thin; the modification necessary to handle the small but finite thickness [11] case is discussed later. To illustrate, the derivation of the spectral Green's function for a stripline filled with a three-layer dielectric [6] is detailed below and only a tabulation of the other spectral Green's functions for the structures considered in this paper is provided later.

Consider the cylindrical stripline shown in Fig. 2 with a three-layer dielectric filling. The potential Ψ in various regions satisfies the Laplace equation [6] in the cylindrical coordinates

$$\nabla_t^2 \Psi = \rho \frac{\partial}{\partial \rho}\left(\frac{\partial \Psi}{\partial \rho}\right) + \frac{\partial^2 \Psi}{\partial \phi^2} = 0. \tag{6}$$

For the case of an infinitely thin strip, the charge distribution assumes the form

$$\sigma(\phi, \rho) = \sigma(\phi)\delta(\rho - d_3) \tag{7}$$

where $\delta(\rho - d_3)$ is the Dirac delta function.

Now define the Fourier transform pair of Ψ via the following integral and summation:

$$\tilde{\Psi}(\rho, n) = \frac{1}{2\pi}\int_0^{2\pi} \Psi(\rho, \phi) e^{jn\phi} d\phi, \qquad 0 < \phi \leqslant 2\pi \tag{8}$$

and

$$\Psi(\rho, \phi) = \sum_{-\infty}^{\infty} \tilde{\Psi}(\rho, n) e^{-jn\phi}. \tag{9}$$

Next, transforming (6) according to (8) gives

$$\left\{-n^2 + \rho \frac{\partial}{\partial \rho}\left(\rho \frac{\partial}{\partial \rho}\right)\right\}\tilde{\Psi}(\rho, n) = 0$$

or

$$\frac{1}{\rho}\frac{d}{d\rho}\rho\frac{d}{d\rho}\tilde{\Psi}(\rho, n) - \frac{n^2}{\rho^2}\tilde{\Psi}(\rho, n) = 0. \tag{10}$$

The boundary and continuity conditions in the Fourier transform domain read

$$\tilde{\Psi}_{\mathrm{III}}(d_4, n) = 0 \tag{11}$$

$$\tilde{\Psi}_{\mathrm{II}}(d_3, n) = \tilde{\Psi}_{\mathrm{III}}(d_3, n) \tag{12}$$

$$\epsilon_{r3}\frac{\partial}{\partial \rho}\tilde{\Psi}_{\mathrm{III}}(d_3, n) = \epsilon_{r2}\frac{\partial}{\partial \rho}\tilde{\Psi}_{\mathrm{II}}(d_3, n) - \frac{1}{\epsilon_0}\tilde{\sigma}(n) \tag{13}$$

$$\tilde{\Psi}_{\mathrm{II}}(d_2, n) = \tilde{\Psi}_{\mathrm{I}}(d_2, n) \tag{14}$$

$$\epsilon_{r2}\frac{\partial}{\partial \rho}\tilde{\Psi}_{\mathrm{II}}(d_2, n) = \epsilon_{r1}\frac{\partial}{\partial \rho}\tilde{\Psi}_{\mathrm{I}}(_2, n) \tag{15}$$

and

$$\tilde{\Psi}_{\mathrm{I}}(d_1, n) = 0 \tag{16}$$

where ϵ_{r1}, ϵ_{r2}, and ϵ_{r3} are the relative dielectric constants for regions I, II, and III, respectively.

In all three regions, the general solution of (10) is $A\ln\rho + B$ for $n=0$ and $A\rho^{-n} + B\rho^{n}$ for $n\neq 0$, respectively. Upon writing these solutions for different regions and enforcing the boundary and continuity conditions (11)–(16), a set of inhomogeneous simultaneous equations for the coefficients of the potential function in the different regions is obtained. These equations are readily solved to yield $\tilde{\Psi}$, the Fourier transform of the potential distribution at $\rho = d_3$. It is given by

$$\tilde{\Phi}(d_3, n) = \tilde{G}(d_3, n)\tilde{\sigma}(n) \tag{17}$$

with

$$\tilde{G}(d_3,0) = \frac{d_3}{\epsilon_0}\frac{N_0}{D_0} \tag{18a}$$

$$\tilde{G}(d_3, n) = \frac{-d_3}{\epsilon_0}\frac{N_n}{D_n} \qquad \text{for } n\neq 0 \tag{18b}$$

where

$$N_0 = \ln\left(\frac{d_3}{d_4}\right)\left\{\epsilon_{r1}\ln\left(\frac{d_2}{d_3}\right) + \epsilon_{r2}\ln\left(\frac{d_1}{d_2}\right)\right\} \tag{19a}$$

$$D_0 = -\epsilon_{r2}\epsilon_{r1}\ln\left(\frac{d_3}{d_4}\right) + \epsilon_{r3}\epsilon_{r1}\ln\left(\frac{d_2}{d_3}\right) + \epsilon_{r2}\epsilon_{r3}\ln\left(\frac{d_1}{d_2}\right) \tag{19b}$$

$$N_n = \epsilon_{r2}\coth\left(|n|\ln\left(\frac{d_2}{d_3}\right)\right) + \epsilon_{r1}\coth\left(|n|\ln\left(\frac{d_1}{d_2}\right)\right) \tag{19c}$$

and

$$\begin{aligned} D_n = |n|\Bigg(&\epsilon_{r3}\epsilon_{r2}\coth\left(|n|\ln\left(\frac{d_3}{d_4}\right)\right)\coth\left(|n|\ln\left(\frac{d_2}{d_3}\right)\right) \\ &+ \epsilon_{r3}\epsilon_{r1}\coth\left(|n|\ln\left(\frac{d_1}{d_2}\right)\right)\coth\left(|n|\ln\left(\frac{d_3}{d_4}\right)\right) \\ &+ \epsilon_{r2}\epsilon_{r1}\coth\left(|n|\ln\left(\frac{d_1}{d_2}\right)\right)\coth\left(|n|\ln\left(\frac{d_2}{d_3}\right)\right) + \epsilon_{r2}^2\Bigg). \end{aligned} \tag{19d}$$

It is important to point out that due to the ϕ periodicity of the cylindrical structure, the spectral Green's function is discrete. Furthermore, the spectral Green's function is symmetric in n. Putting $\epsilon_{r1} = \epsilon_{r2} = \epsilon_{r3}$, we have the spectral Green's function for the single dielectric stripline described in [1]–[6].

The spectral Green's function for the microstrip line discussed in [1] and [5] can be obtained easily by setting $\epsilon_{r1} = \epsilon_{r2} = \epsilon_{r3}$ and $d_4 \to \infty$. The resulting equation is given as

$$\tilde{G}(d_3,0) = \frac{d_3}{\epsilon_0\epsilon_{r1}}\ln\left(\frac{d_3}{d_1}\right) \tag{20a}$$

and

$$\tilde{G}(d_3, n) = \frac{-d_2\coth\left(|n|\ln\left(\frac{d_1}{d_3}\right)\right)}{|n|\epsilon_0\left(-\coth\left(|n|\ln\left(\frac{d_1}{d_3}\right)\right) + \epsilon_{r1}\right)} \qquad \text{for } n\neq 0. \tag{20b}$$

If the conducting strips are placed at $\rho = d_2$, $\epsilon_{r3} = 1$, and $d_4 \to \infty$, the buried microstrip configuration is obtained. Again, for $\epsilon_{r2} = \epsilon_{r1}$, we have

$$\tilde{G}(d_2,0) = \frac{d_2\ln\left(\frac{d_2}{d_1}\right)}{\epsilon_{r1}\epsilon_0} \tag{21a}$$

and

$$\begin{aligned} \tilde{G} = &\frac{-d_2\cosh\left(|n|\ln\left(\frac{d_1}{d_2}\right)\right)}{2|n|\epsilon_{r1}\epsilon_0} \\ &\cdot\left\{\frac{-\cosh\left(|n|\ln\left(\frac{d_2}{d_3}\right)\right) + \epsilon_{r1}\sinh\left(|n|\ln\left(\frac{d_2}{d_3}\right)\right)}{-\cosh\left(|n|\ln\left(\frac{d_1}{d_3}\right)\right) + \epsilon_{r1}\sinh\left(|n|\ln\left(\frac{d_1}{d_3}\right)\right)}\right\} \end{aligned} \qquad \text{for } n\neq 0. \tag{21b}$$

If we place another set of conducting strips at $\rho = d_2$ (see Fig. 1), we obtain a different coupled stripline system. To derive the spectral Green's function of this new structure, we simply replace $\tilde{\sigma}$ in (13) by $\tilde{\sigma}_1$. At the interface between regions I and II, (15) is replaced by the new boundary condition, which reads

$$\epsilon_{r2}\frac{\partial}{\partial\rho}\Psi_{\mathrm{II}}(d_2, n) = \epsilon_{r1}\frac{\partial}{\partial\rho}\tilde{\Psi}_{\mathrm{I}}(d_2, n) - \frac{1}{\epsilon_0}\tilde{\sigma}_2(n). \tag{22}$$

Here, $\tilde{\sigma}_1$ and $\tilde{\sigma}_2$ are the Fourier transforms of the charge distributions at $\rho = d_3$ and d_2, respectively. Solving the algebraic equations, we obtain

$$\begin{bmatrix}\Psi_{\mathrm{III}}(d_3, n)\\ \Psi_{\mathrm{II}}(d_2, n)\end{bmatrix} = \begin{bmatrix}\tilde{G}_{11}(n) & \tilde{G}_{12}(n)\\ \tilde{G}_{21}(n) & \tilde{G}_{22}(n)\end{bmatrix}\begin{bmatrix}\tilde{\sigma}_1(n)\\ \tilde{\sigma}_2(n)\end{bmatrix} \tag{23}$$

where

$$\tilde{G}_{11}(0) = d_3\ln\left(\frac{d_3}{d_4}\right)\left[\epsilon_{r1}\ln\left(\frac{d_3}{d_2}\right) + \epsilon_{r2}\ln\left(\frac{d_2}{d_1}\right)\right]\Big/ D(0) \tag{24a}$$

$$\tilde{G}_{12}(0) = \epsilon_{r2}d_2\ln\left(\frac{d_3}{d_1}\right)\ln\left(\frac{d_3}{d_4}\right)\Big/ D(0) \tag{24b}$$

$$\tilde{G}_{21}(0) = \epsilon_{r2}d_3\ln\left(\frac{d_2}{d_1}\right)\ln\left(\frac{d_3}{d_4}\right)\Big/ D(0) \tag{24c}$$

$$\tilde{G}_{22}(0) = d_2\ln\left(\frac{d_2}{d_1}\right)\left[\epsilon_{r2}\ln\left(\frac{d_3}{d_4}\right) + \epsilon_{r3}\ln\left(\frac{d_2}{d_3}\right)\right]\Big/ D(0) \tag{24d}$$

$$\tilde{G}_{11}(n) = -d_3 \sinh\left(|n|\ln\left(\frac{d_4}{d_3}\right)\right)\left[\epsilon_{r2}\cosh\left(|n|\ln\left(\frac{d_2}{d_3}\right)\right)\sinh\left(|n|\ln\left(\frac{d_2}{d_1}\right)\right) - \epsilon_{r1}\cosh\left(|n|\ln\left(\frac{d_2}{d_1}\right)\right)\sinh\left(|n|\ln\left(\frac{d_2}{d_3}\right)\right)\right] \Big/ D(n) \tag{25a}$$

$$\tilde{G}_{12}(n) = -2\epsilon_{r2}d_2 \sinh\left(|n|\ln\left(\frac{d_4}{d_3}\right)\right)\sinh\left(|n|\ln\left(\frac{d_2}{d_1}\right)\right) \Big/ D(n) \tag{25b}$$

$$\tilde{G}_{21}(n) = -2\epsilon_{r2}d_3 \sinh\left(|n|\ln\left(\frac{d_4}{d_3}\right)\right)\sinh\left(|n|\ln\left(\frac{d_2}{d_1}\right)\right) \Big/ /D(n) \tag{25c}$$

$$\tilde{G}_{22}(n) = -d_2 \sinh\left(|n|\ln\left(\frac{d_2}{d_1}\right)\right)\left[\epsilon_{r2}\sinh\left(|n|\ln\left(\frac{d_4}{d_3}\right)\right)\cosh\left(|n|\ln\left(\frac{d_2}{d_3}\right)\right) - \epsilon_{r3}\cosh\left(|n|\ln\left(\frac{d_4}{d_3}\right)\right)\sinh\left(|n|\ln\left(\frac{d_2}{d_3}\right)\right)\right] \Big/ D(n) \tag{25d}$$

where

$$D(0) = \epsilon_0\left(\epsilon_{r1}\epsilon_{r3}\ln\left(\frac{d_2}{d_3}\right) + \epsilon_{r1}\epsilon_{r2}\ln\left(\frac{d_3}{d_4}\right) + \epsilon_{r2}\epsilon_{r3}\ln\left(\frac{d_1}{d_2}\right)\right) \tag{26a}$$

$$\begin{aligned} D(n) = |n|\epsilon_0\Bigg(&\epsilon_{r2}^2\sinh\left(|n|\ln\left(\frac{d_2}{d_3}\right)\right)\sinh\left(|n|\ln\left(\frac{d_4}{d_3}\right)\right)\sinh\left(|n|\ln\left(\frac{d_2}{d_1}\right)\right) \\ &- \epsilon_{r2}\epsilon_{r3}\cosh\left(|n|\ln\left(\frac{d_2}{d_3}\right)\right)\cosh\left(|n|\ln\left(\frac{d_4}{d_3}\right)\sinh\left(|n|\ln\left(\frac{d_2}{d_1}\right)\right)\right) \\ &- \epsilon_{r1}\epsilon_{r2}\cosh\left(|n|\ln\left(\frac{d_2}{d_1}\right)\right)\cosh\left(|n|\ln\left(\frac{d_2}{d_3}\right)\right)\sinh\left(|n|\ln\left(\frac{d_4}{d_3}\right)\right) \\ &+ \epsilon_{r1}\epsilon_{r3}\sinh\left(|n|\ln\left(\frac{d_2}{d_3}\right)\right)\cosh\left(|n|\ln\left(\frac{d_4}{d_3}\right)\right)\cosh\left(|n|\ln\left(\frac{d_2}{d_1}\right)\right)\Bigg). \end{aligned} \tag{26b}$$

If we let $d_4 \to \infty$, we can obtain the spectral Green's function for the case where we have a layer of microstrip lines and a layer of buried microstrip lines.

The deviations of the above spectral Green's functions were based on the assumption that the thickness of the strip is negligible compared to the arc length of the strip. When the strip has a finite thickness, we need to modify the spectral Green's function. As an example, the case of a single-dielectric-layer stripline of finite thickness [5] is discussed here.

In the derivation of the spectral Green's function for the case of an infinitely thin strip, the constants for the general solutions of (6) are evaluated. Substituting these constants into the representation of the potential function in region III, the potential at a small distance δ above the strip at $\rho = d_3$ is related to the potential at $\rho = d_3$ by

$$\Psi(d_3+\delta,0) = \frac{\ln\left(\frac{d_3+\delta}{d_4}\right)}{\ln\left(\frac{d_3}{d_4}\right)}\Psi(d_3,0) \tag{27a}$$

and

$$\Psi(d_3+\delta,n) = \frac{\sinh\left(|n|\ln\left(\frac{d_3+\delta}{d_4}\right)\right)}{\sinh\left(|n|\ln\left(\frac{d_3}{d_4}\right)\right)} \quad \text{for} \quad n \neq 0. \tag{27b}$$

Considering the two layers of charge at $d_3+\delta$ and d_3, with each having the same amount of total charge, the spectral Green's function can be modified by multiplying by the correcting function

$$\Gamma(0) = \left(1 + \frac{\ln\left(\frac{d_3+\delta}{d_4}\right)}{\ln\left(\frac{d_3}{d_4}\right)}\right) \Big/ 2 \tag{28a}$$

and

$$\Gamma(n)=\left(1+\frac{\sinh\left(|n|\ln\left(\frac{d_3+\delta}{d_4}\right)\right)}{\sinh\left(|n|\ln\left(\frac{d_3}{d_4}\right)\right)}\right)\Bigg/2 \quad \text{for} \quad n\neq 0. \tag{28b}$$

Since the charges at the two edges are neglected, this approximation is valid only for a small ratio of finite thickness to the arc length of the conducting strips. For the cylindrical stripline, the results are compared with the thick-strip results calculated from the equations given in [5].

IV. The Iterative Procedure

An iterative algorithm based on that in [7] and [9] for solving (1) is constructed by defining an error criterion as follows:

$$F(\phi)=V(\phi)-\int_D G(\phi,\phi')\sigma'(\phi')d\phi' \tag{29}$$

$$\text{BCE}=\left\{\frac{\int_D|F(\phi)|^2\rho d\phi}{\int_D|V(\phi)|^2\rho d\phi}\right\}^{1/2} \tag{30}$$

where σ' represents an initial guess, and BCE denotes the boundary condition error. The updated σ is generated and is used as the initial guess for the subsequent iteration. This procedure systematically and monotonically improves the accuracy of the solution and is repeated until the error is sufficiently small [7]–[9].

The convolution operation in (1) with the ρ dependence suppressed is carried out in the following manner:

$$\int_D G(\phi,\phi')\sigma'(\phi')d\phi'=F^{-1}\{\tilde{G}\cdot F[\sigma']\} \tag{31}$$

where F and F^{-1} represent forward and inverse Fourier transforms, respectively.

The present method is slightly different from those in [7]–[9] in that the δ sampling is not used in discretizing the continuous function σ. Instead, we expand the unknown function σ by cylindrical pulses as follows:

$$\sigma(\phi)=\sum_{-N/2}^{N/2-1}\sigma_n P_n \tag{32}$$

where

$$P_n=\begin{cases}1 & \text{if } \left(n-\frac{1}{2}\right)\Delta\phi\leqslant\phi\leqslant\left(n+\frac{1}{2}\right)\Delta\phi\\ 0 & \text{otherwise}\end{cases} \tag{33}$$

$$\Delta\phi=\frac{2\pi}{N} \tag{34}$$

$$\sigma_n=0 \quad \text{when} \quad \phi\notin D. \tag{35}$$

The reason for using the cylindrical pulse function, as opposed to δ sampling, is that the convergence of the iterative procedure is usually superior for the pulse expansion relative to the δ-sampling case. Upon Fourier-transforming (32), we obtain

$$\tilde{\sigma}=\text{sinc}\left(\frac{n\Delta\phi}{2}\right)\text{FFT}(\sigma_n) \tag{36a}$$

or

$$\tilde{\sigma}=\tilde{S}\,\text{FFT}(\sigma_n). \tag{36b}$$

Hence, the continuous convolution in (1) can be written as a discrete convolution:

$$\int_D G(\phi,\phi')\sigma'(\phi')\,d\phi'=\text{FFT}^{-1}\left\{\tilde{G}\cdot\text{sinc}\frac{n\Delta\phi}{2}\,\text{FFT}(\sigma')\right\}. \tag{37}$$

The modified algorithm is given as

****

$$k=0 \quad \sigma_n^0=0 \tag{38}$$

$$F_n^0=V_n \tag{39}$$

$$\text{BCE}\,N=\sum_{-N/2}^{N/2-1}|V_n|\rho\Delta\phi \tag{40}$$

$$\text{BCE}^0=1 \tag{41}$$

****

$$k=k+1 \quad g_n^k=\text{FFT}^{-1}\left(\text{FFT}\left(F_n^{k-1}\right)\tilde{S}_n\tilde{G}_n^{-1}\right) \tag{42}$$

$$f_n^k=\text{FFT}^{-1}\left(\text{FFT}\left(g_n^k\right)\tilde{S}_n\tilde{G}_n\right) \tag{43}$$

$$A^k=\sum_{-N/2}^{N/2-1}F_n^{(k-1)*}f_n^k\rho\Delta\phi \tag{44}$$

$$B^k=\sum_{-N/2}^{N/2-1}|f_n^k|\rho\Delta\phi \tag{45}$$

****

$$\text{if } n>1 \quad C^k=\sum_{-N/2}^{N/2-1}f_n^{k*}f_n^{k-1}\rho\Delta\phi \tag{46}$$

$$\zeta^k=C^{k*}/B^{k-1} \tag{47}$$

$$B^k=B^k-\zeta^kC^k \tag{48}$$

$$g_n^k=g_n^k-\zeta^kg_n^{k-1} \tag{49}$$

$$f_n^k=f_n^k-\zeta^kf_n^{k-1} \tag{50}$$

$$\eta^k=a^{k*}/B^k \tag{51}$$

$$\sigma_n^k=\sigma_n^{k-1}+\eta^kg_n^k \tag{52}$$

$$F_n^k=F_n^{k-1}-\eta^kf_n^k \tag{53}$$

$$\text{BCE}^k=\left\{\frac{\sum_{-N/2}^{N/2-1}|F_n^k|^2\rho\Delta\phi}{\text{BCE}\,N}\right\}^{1/2}. \tag{54}$$

The asterisk represents the complex conjugate operation.

****

There are several important features of the iterative approach, as enumerated below. First, this iterative process generates a numerically rigorous solution to the discretized problem and does not involve the truncation of the infinite series as in [1] and [6]. Second, it can have a large number of unknowns without suffering from the computer storage problem, as in the matrix methods, because the iterative algorithm only requires the storage of column vectors. Third, the iteration process typically converges very quickly[1] and can be terminated once the desired accuracy is reached. Fourth, the choice of the initial guess σ' is not critical; in fact, it can even be zero. Fifth, in contrast to the matrix or dual series approach, the accuracy of the results can be readily improved in the iterative procedure by simply increasing the number of expansion pulses without increasing the complexity of the computational steps. Finally, the algorithm is easy to program and different structures can be analyzed by simply changing the spectral Green's function subroutine.

V. Numerical Results

A number of cylindrical multiconductor transmission lines have been investigated using this iterative method and some representative results are presented in this paper. For further details, the reader is referred to Chan and Mittra [15]. Since the iterative method is solving an approximate problem in which continuous functions are being approximated by series of cylindrical pulses, it is necessary to verify the numerical convergence by increasing the number of these pulse functions and studying the behavior of the solution. Table I shows the normalized characteristic impedance of a homogeneous stripline with $\epsilon_{r1} = \epsilon_{r2} = \epsilon_{r3}$, $d_4/d_1 = 2$, $d_3/d_1 = 1.8$, and $d_2/d_1 = 1.4$. Three different sampling rates $\Delta\delta = 2\pi/N$ with $N = 512$, 1024, and 2048 are used. The stopping criterion of the iteration process is set at BCE $\leqslant 5 \times 10^{-4}$. It took seven iterations at most and about 4 s on a VAX 11/780 for $N = 2048$. For $N = 512$, it usually took only three to five iterations and fractions of a second to stop the iteration process. Because of numerical discretization, the width of the strip must be a multiple of $2\pi/2^m$ for applying the radix 2 FFT. Hence, the strip half-angle is slightly different for the three different sampling rates. Keeping this in mind, we note that, in general, the solutions agree very well with each other, and we conclude that $N = 512$ is adequate for achieving numerical convergence. Consequently, for the rest of the calculations, $N = 512$ is assumed.

For the thin dielectric case, i.e., when $d_4/d_1 = 1.1$, the approximation used in [1] and [6] is valid and the results compare well with the iterative method shown in Fig. 3. For a thicker dielectric, i.e., for $d_4/d_1 = 2$ and $d_3/d_1 = 1.8$, the results from [1] and [6] seem to be somewhat inaccurate when the strip half-angle is less than 80°. However, for $d_3/d_1 = 1.4$, a reasonably good approximate solution is obtained if the effective strip half-angle [6] is used. The results for $d_4/d_1 = 2$ are shown in Figs. 4 and 5. Table II shows the results for a homogeneous stripline of two different thicknesses obtained by [5], [6] and the present method. For $d_4/d_1 = 2$, good agreement is obtained. However, for $d_4/d_1 = 6$, while the results from [5] and the present method agree to within 0.5 percent, the results calculated from [6] are erroneous. Hence, the accuracy of the results shown in [6, figs. 11–16] is questionable.

[1] The nondivergence of the iterations scheme has been proved in [7] and [14].

TABLE I
Normalized Characteristic Impedance of a Homogeneous Stripline as a Function of Strip Half-Angle with Different Sampling Rates

N = 512		N = 1024		N = 2048	
α	$\sqrt{\epsilon_{r1}} Z_0$ (ohms)	α	$\sqrt{\epsilon_{r1}} Z_0$ (ohms)	α	$\sqrt{\epsilon_{r1}} Z_0$ (ohms)
20 04	38.23	19 86	38 32	19 95	38.14
39 73	21 43	39 90	21 33	39.99	21.27
60.12	14.75	59 94	14 78	60 03	14 75
79.82	11.34	79.98	11.31	80 07	11 29
100.20	9 14	100.02	9.16	99.93	9 16
119.88	7 71	120 06	7.69	119.97	7.70
140.27	6.63	140.10	6.63	140.01	6.64

$\epsilon_{r1} = \epsilon_{r2} = \epsilon_{r3}$, $d_4/d_1 = 2$, $d_3/d_1 = 1.8$, and $d_2/d_1 = 1.4$.

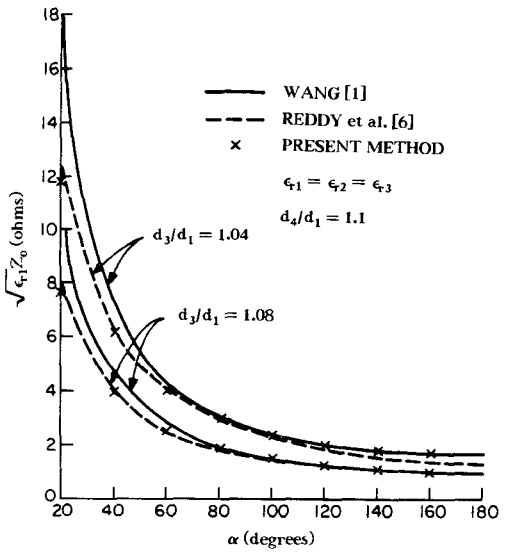

Fig. 3. Normalized characteristic impedance of a homogeneous cylindrical stripline as a function of strip half-angle.

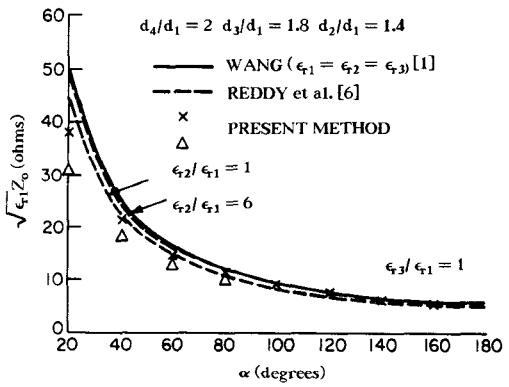

Fig. 4. Normalized characteristic impedance of a three-layer dielectric-filled stripline as a function of strip half-angle.

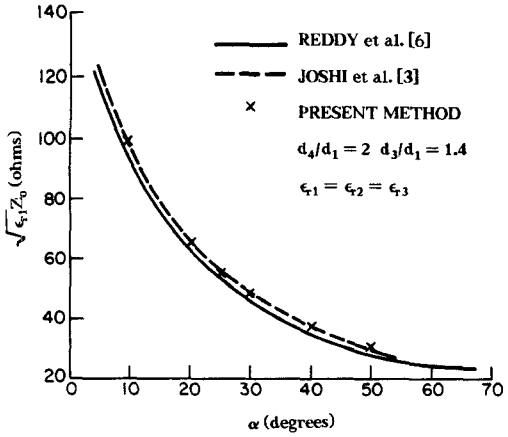

Fig. 5. Normalized characteristic impedance of a homogeneous stripline as a function of strip half-angle.

TABLE II
NORMALIZED CHARACTERISTIC IMPEDANCE OF A HOMOGENEOUS STRIPLINE AS A FUNCTION OF STRIP HALF-ANGLE CALCULATED FROM THREE DIFFERENT METHODS

α	$\sqrt{\epsilon_{r1}}Z_0$ (ohms) $d_4/d_1=2$. $d_3/d_1=\sqrt{2}$			$\sqrt{\epsilon_{r1}}Z_0$ (ohms) $d_4/d_1=6$, $d_3/d_1=\sqrt{6}$		
	[5]	Present Method	[6] with α_{eff}	[5]	Present Method	[6] with α_{eff}
10.20	98 97	99.53	100.70	153 42	154 06	178.20
20.04	64.93	65.21	65.83	114.21	114.57	130.78
29 88	48.39	48 56	48.90	92.20	92 39	103 30
39 73	38 49	38.68	38 90	77.53	77 72	85 36

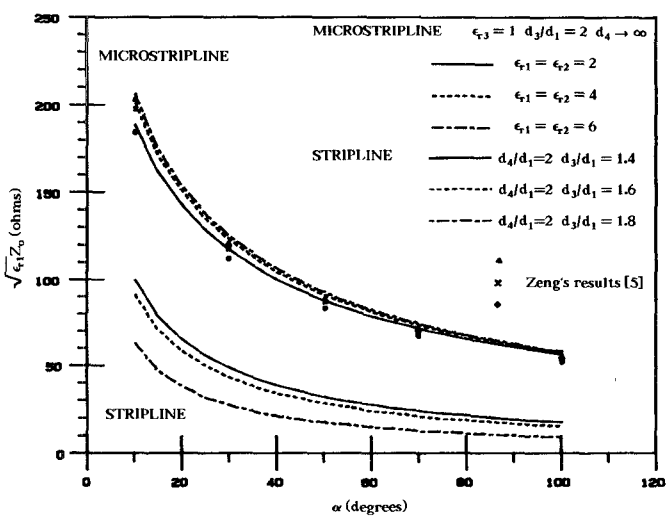

Fig. 6. Normalized characteristic impedances of cylindrical stripline and microstrip line as a function of strip half-angle.

Figs. 6 and 7 show the normalized characteristic impedances of striplines, microstrip lines, and buried microstrip lines. The characteristic impedance is given by $Z_0 = \sqrt{(L/C)}$. The conducting strip is located at $\rho = d_3$, $\rho = d_3$, and $\rho = d_2$ for the stripline, microstrip line, and buried microstrip line, respectively. In Fig. 6, the microstrip line case is compared with the results obtained from the approximate solution given in [5] and good agreement is obtained. In Fig. 7, we varied the distance between the conducting strip and the ground plate at $\rho = d_1$ of the buried microstrip line. As the strip gets closer to the

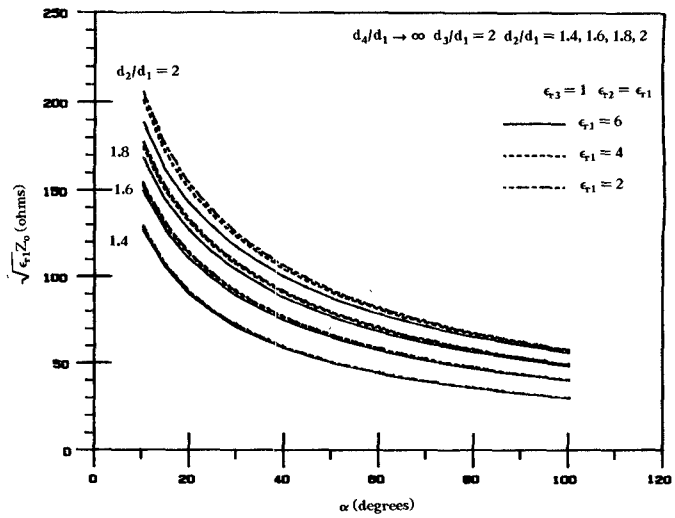

Fig. 7. Normalized characteristic impedance of a buried microstrip line as a function of strip half-angle.

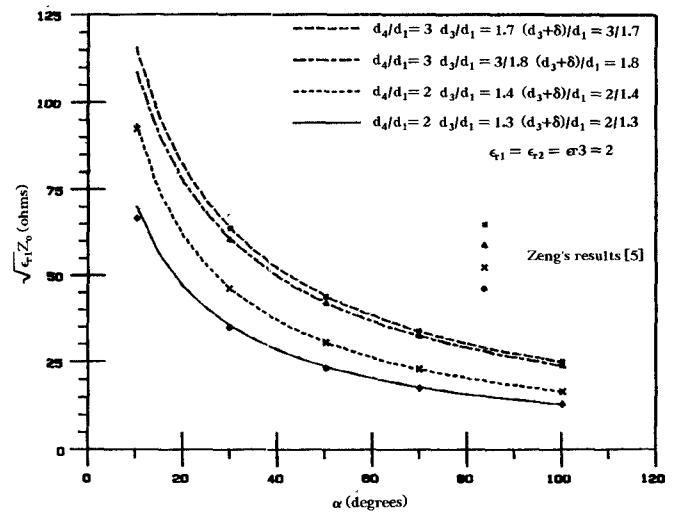

Fig. 8. Normalized characteristic impedance of a homogeneous stripline with finite thickness δ as a function of strip half-angle.

ground plate, the normalized characteristic impedance is affected little by the air region above $\rho = d_3$. As ρ increases, the effect due to different dielectrics becomes stronger. Finally, when $\rho \to d_3$, the buried microstrip line resembles the microstrip line.

The finite-thickness case for the stripline is compared with the results calculated from the equations given in [5]. The parameters are chosen such that (29)–(32) and (27) and (28) in [5] can be used. Equation (27) seems to have a parenthesis missing; the denominator should read $\sqrt{\epsilon_r}(x(W/H)+(1/\pi)P(x))$. The results are shown in Fig. 8 and very good agreement between the present method and [5] is obtained.

The iterative method is next extended to treat two coupled transmission lines. The conducting strips have the same strip half-angle of $\alpha = 10.195°$. The separation angle γ between the strips is defined as in Fig. 9. For two conducting strips of equal strip half-angle α on the same ρ plane, we can define the even- and odd-mode characteristic impedances denoted by Z_{0e} and Z_{0o}, respectively, as in

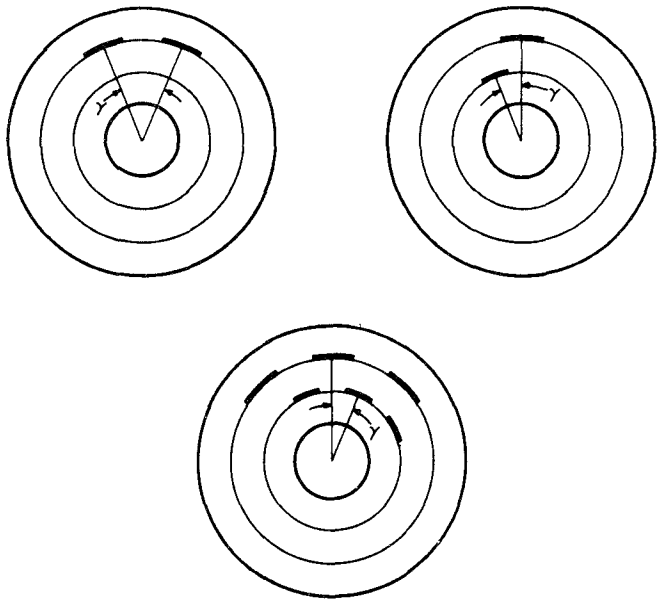

Fig. 9. Definition of angle of separation γ for coupled transmission lines.

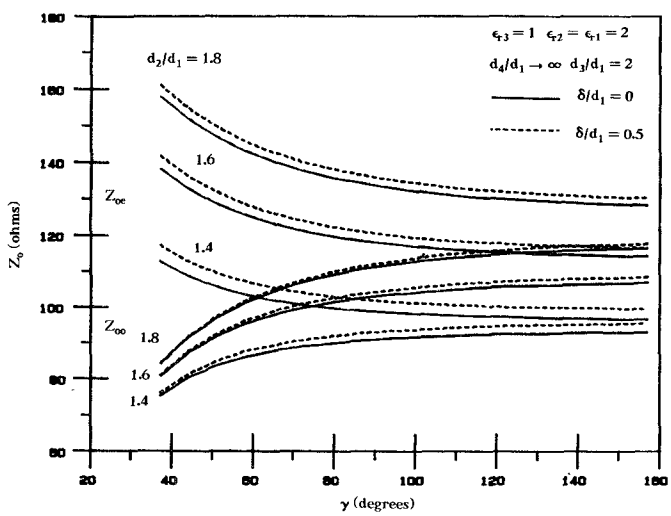

Fig. 10. Even- and odd-mode characteristic impedances of two coupled cylindrical buried microstrip lines as a function of separation angle; $\delta/d_1=0$, 0.5 and $\alpha=10.195°$.

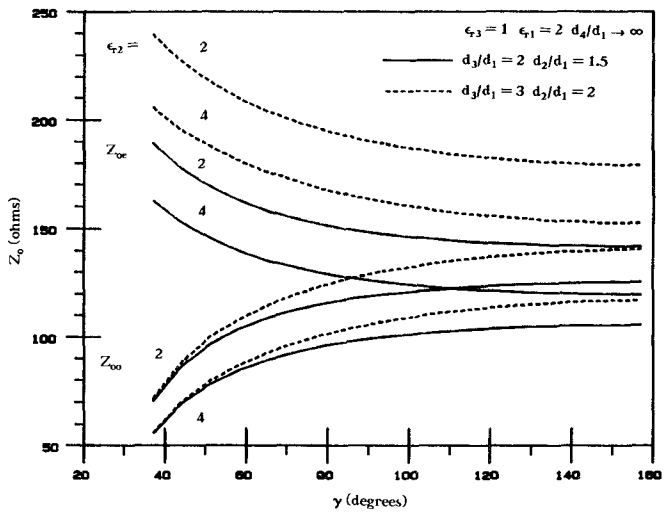

Fig. 11. Even- and odd-mode characteristic impedances of two coupled cylindrical microstrip lines as a function of separation angle; $\alpha=10.195°$.

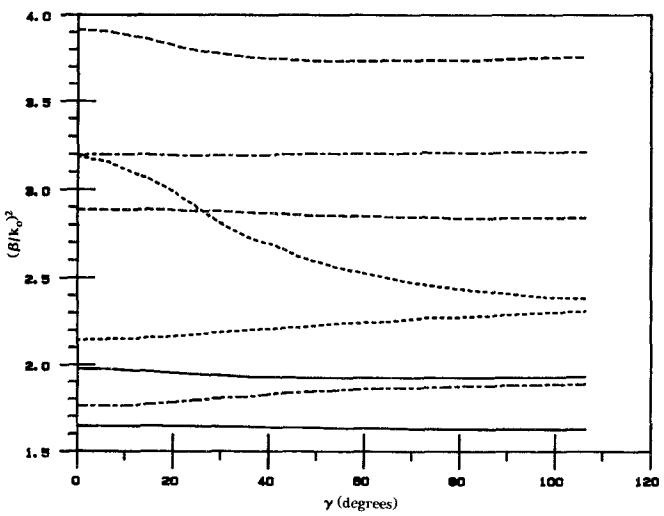

Fig. 12. Variation of propagation constants of a cylindrical microstrip line at $\rho=d_3$ coupled with a buried microstrip line at $\rho=d_2$ as a function of separation angle. ——$\epsilon_{r1}=\epsilon_{r2}=2$; -----$\epsilon_{r1}=2$, $\epsilon_{r2}=4$; – – –$\epsilon_{r1}=4$, $\epsilon_{r2}=2$; – – – – –$\epsilon_{r1}=\epsilon_{r2}=4$. $d_4/d_1\to\infty$, $d_3/d_1=3$, $d_2/d_1=2$, $\epsilon_{r3}=1$, and $\alpha=10.195°$.

[12]. Fig. 10 shows the Z_{0e} and Z_{0o} of two coupled buried microstrip lines of two different thickness, $\delta/d_1=0$ and 0.5, located at $\rho/d_1=1.4$, 1.6, and 1.8 with $\epsilon_{r1}=\epsilon_{r2}=2$. The finite thickness does not have much effect on z_{0o} when the separation angle is small. For smaller d_2/d_1, Z_{0e} and Z_{0o} approach each other as the separation angle between the strips increases; this means that when the strips are closer to d_1, the coupling between the strips is less for larger γ, because the fields are confined to the strips. Increases in d_2/d_1 result in an increase in Z_{0e} but a decrease in Z_{0o}. Fig. 11 shows Z_{0e} and Z_{0o} of two coupled microstrip lines of two dielectric layers. Increases in d_3/d_1 will increase both Z_{0e} and Z_{0o}. Increases in the dielectric constant in region II will decrease both Z_{0e} with Z_{0o}. The coupling between the microstrip lines is stronger than that for the buried microstrip case as the differences between Z_{0e} and Z_{0o} are larger for large γ. Although not shown here, Z_{0e} and Z_{0o} for a coupled stripline with a three-layer dielectric decrease when the dielectric constants increase [15]. Unlike the buried microstrip or the microstrip case, Z_{0e} and Z_{0o} of the coupled striplines are equal at large γ, which implies that the coupling between two strips diminishes as γ increases.

When the two coupled transmission lines lie on two different ρ planes, we cannot define the even- and odd-mode characteristic impedances for the coupled system. Instead, we calculated the propagation constant β of each of the two propagating modes. These propagation constants can be converted into effective dielectric constants for the propagating modes. Fig. 12 shows the variation of the effective dielectric constant $(\beta/k_0)^2$ with γ for two

TABLE III
EFFECTIVE DIELECTRIC CONSTANTS OF SIX COUPLED STRIPLINES AS A FUNCTION OF SEPARATION ANGLE

separation angle γ (degrees)	effective dielectric constant					
	1 st mode	2 nd mode	3 rd mode	4 th mode	5 th mode	6 th mode
0 00	3.0277	3.0759	3.1405	5.0790	5.1479	5.2594
6.33	3.0294	3.0777	3.1413	5.0761	5.1457	5.2582
18.98	3.0362	3.0858	3.1489	5.0619	5.1305	5.2508
35.86	3.0305	3.0873	3.1622	5.0663	5.1240	5.2470
63 98	3.0370	3 0885	3.1873	5.0576	5.1133	5.2221
106.17	3.0372	3.1004	3.2147	5.0562	5.1103	5.1854

$d_4/d_1 = 4$, $d_3/d_1 = 3$, $d_2/d_1 = 2$, $\alpha = 10.195°$, $\epsilon_{r1} = 2$, $\epsilon_{r2} = 4$, $\epsilon_{r3} = 6$.

TABLE IV
EFFECTIVE DIELECTRIC CONSTANTS OF THREE MICROSTRIP LINES COUPLED WITH THREE BURIED MICROSTRIP LINES AS A FUNCTION OF SEPARATION ANGLE

separation angle γ (degrees)	effective dielectric constant					
	1 st mode	2 nd mode	3 rd mode	4 th mode	5 th mode	6 th mode
0.00	2.0722	2.1945	2.3896	3.0725	3.1504	3.4138
6.33	2.0723	2.1987	2.3982	3.0551	3.1382	3.4092
18.98	2.0749	2.2251	2.4461	2.9133	3.0722	3.3689
35.86	2.0768	2 2354	2.4215	2.6929	3.1001	3.3641
63.98	2.0833	2.2860	2.4021	2.5362	2.9412	3.2611
106.17	2.1075	2.2978	2.3393	2.4311	2.7887	3.0065

$d_4/d_1 \to \infty$, $d_3/d_1 = 3$, $d_2/d_1 = 2$, $\epsilon_{r1} = 2$, $\epsilon_{r2} = 4$, $\epsilon_{r3} = 1$, and $\alpha = 10.195°$.

coupled strips located at $\rho = d_2$ and d_3, respectively, for $\epsilon_{r3} = 1$ and $d_4 \to \infty$. The variation in β as a function of γ is considerably more pronounced for this configuration than for homogeneously filled coupled striplines [15]. For the coupled stripline, the two propagation constants coalesce and $(\beta/k_0)^2$ is simply equal to the dielectric constant.

For the cylindrical multiconductor transmission line, we first treat a stripline structure with two layers of strips located at $\rho = d_3$ and $\rho = d_2$, respectively. Each layer of strip consists of three strips. Each strip has a strip half-angle of 10.195° and the strips on the same ρ plane are 20.39° apart. As a second example, we treat a combined microstrip and buried microstrip structure by setting $\epsilon_{r3} = 1$ and $d_4 \to \infty$. To calculate the propagation constants of the propagating modes, we need $[L]$ and $[C]$ matrices. To obtain $[L]$ or $[C]$ matrices, we need to solve (1) for six independent excitations. In general, it took about seven to ten iterations for each excitation. The CPU time on a VAX 11/780 for computing six excitations is about 4–5 seconds. Table III shows how the six propagating modes of the coupled stripline system vary with the separation angle γ. The propagation constants of the six propagating modes do not vary too much as γ increases, and they cluster into two groups due to the fact that the two sets of strips lie on two different planes. Table IV shows the six propagating modes of the combined microstrip and buried microstrip structure. The propagation constants have a larger variation as γ increases. It is found that the larger the discontinuities in the dielectric-to-dielectric and dielectric-to-air interfaces, the larger the variation of β with γ.

VI. CONCLUSIONS

A class of cylindrical multiconductor transmission lines has been analyzed by a numerically rigorous iterative procedure. Because of the periodicity of the cylindrical structure, numerical efficiency can be obtained via the use of FFT. The numerical results are compared with available data. Results from the present method compare well with those obtained by conformal mapping; however, we also find that results generated using the series expansion method [1], [5] can be in error if a sufficient number of terms are not included. Extensive data on different cylindrical structures have been presented to illustrate the versatility of the present method. Finally, the method is suitable for treating multiple lines by simply increasing the sampling rate.

REFERENCES

[1] Y. C. Wang, "Cylindrical and cylindrically warped strip and microstrip lines," *IEEE Trans. Microwave Theory Tech.*, vol. MTT-26, pp. 20–23, Jan. 1978.

[2] K. K. Joshi and B. N. Das, "Analysis of elliptic and cylindrical striplines using Laplace's equation," *IEEE Trans. Microwave Theory Tech.*, vol. MTT-28, pp. 381–386, May 1980.

[3] K. K. Joshi, J. S. Rao, and B. N. Das, "Characteristic impedance of nonplanar striplines," *Proc. Inst. Elec. Eng.*, Pt. H, vol. 127, pp. 287–291, Aug. 1980.

[4] B. N. Das, A. Chakrabarty, and K. K. Joshi, "Characteristic impedance of elliptic cylindrical strip and microstrip lines filled with layered substrate," *Proc. Inst. Elec. Eng.*, Pt. H, vol. 130, pp. 245–250, June 1983.

[5] L. R. Zeng and Y. X. Wang, "Accurate solutions of elliptical and cylindrical striplines and microstrip lines," *IEEE Trans. Microwave Theory Tech.*, vol. MTT-34, pp. 259–265, Feb. 1986.

[6] C. J. Reddy and M. D. Deshpande, "Analysis of cylindrical stripline with mutilayer dielectrics," *IEEE Trans. Microwave Theory Tech.*, vol. MTT-34, pp. 701–706, June 1986.

[7] P. M. van den Berg, "Iterative computational techniques in scattering based upon the integrated square error criterion," *IEEE Trans. Antennas Propagat.*, vol. AP-32, pp. 1063–1071, Oct. 1984.

[8] C. Chan and R. Mittra, "Spectral iterative techniques for analyzing multiconductor microstrip lines," in *IEEE MTT Symp. Dig.*, May 1984, pp. 463–465.

[9] RT. Mittra and C. H. Chan, "Iterative approaches to the solution of electromagnetic boundary value problems," *Electromagnetics*, vol. 5, nos. 2–3, pp. 123–146, 1985.

[10] T. A. Cwik, "Scattering from general periodic screens," Ph.D. dissertation, University of Illinois, Urbana, IL, 1986.

[11] E. Yamashita and R. Mittra, "Variational method for the analysis of microstrip lines," *IEEE Trans. Microwave Theory Tech.*, vol. MTT-16, pp. 251–256, Apr. 1986.

[12] Y. Rahmat-Samii, T. Itoh, and R. Mittra, "A spectral domain technique for solving coupled microstrip line problems," *Arch. Elek. Übertragung*, Band 27, pp. 69–71, 1973.

[13] C. Wei *et al.*, "Multiconductor transmission lines in multilayered dielectric media," *IEEE Trans. Microwave Theory Tech.*, vol. MTT-32, pp. 439–449, Apr. 1984.

[14] P. M. van den Berg, "Iterative schemes based on the minimization of the error in field problems," *Electromagnetics*, vol. 5, nos. 2–3, pp. 237–262, 1985.

[15] C. H. Chan and R. Mittra, "Analysis of a class of cylindrical multiconductor transmission lines using an iterative approach," Electromagnetic Communication Lab. Rep., University of Illinois, Urbana, IL, 1986.

Chi Hou Chan (S'86–M'87) was born in Macao on April 16, 1959. He attended Hong Kong Polytechnic and the City College of New York. He received the B.S. and M.S. degrees in electrical engineering

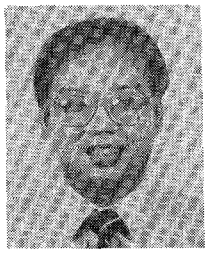

from the Ohio State University, Columbus, OH, in 1981 and 1982, respectively. He is currently pursuing the Ph.D. degree at the University of Illinois at Urbana.

From 1981 to 1982, he was a Graduate Research Associate at the ElectroScience Laboratory, Ohio State University. Presently, he is a Graduate Research Assistant with the Electromagnetic Communication Laboratory in the Department of Electrical and Computer Engineering at the University of Illinois. His research interests include numerical techniques in electromagnetics, scattering from electrically large bodies, frequency-selective surfaces, microwave integrated circuits, high-speed digital circuits, and integrated optics.

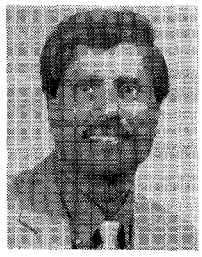

Raj Mittra (S'54–M'57–SM'69–F'71) is the Director of the Electromagnetic Communication Laboratory of the Electrical and Computer Engineering Department and Research Professor of the Coordinated Science Laboratory at the University of Illinois. He is a former president of the IEEE Antennas and Propagation Society. He serves as a consultant to several industrial and governmental organizations in the United States and abroad.

His professional interests include the areas of analytical and computer-aided electromagnetics, high-speed digital circuits, radar scattering, satellite antennas, microwave and millimeter-wave integrated circuits, frequency-selective surfaces, EMP and EMC analysis, and interaction of electromagnetic waves with biological media.